2014

Improved Rotor Position and Speed Estimators for Sensorless Control of Interior Permanent-Magnet Synchronous Machines

Yue Zhao
University of Nebraska-Lincoln, yue.zhao@huskers.unl.edu

Wei Qiao
University of Nebraska-Lincoln, wqiao@engr.unl.edu

Long Wu
John Deere Electronic Solutions, Fargo, ND, WuLong@JohnDeere.com

Pages: 627 - 639, DOI: 10.1109/JESTPE.2014.2298433

Improved Rotor Position and Speed Estimators for Sensorless Control of Interior Permanent-Magnet Synchronous Machines

Yue Zhao, *Student Member, IEEE*, Wei Qiao, *Senior Member, IEEE*, and Long Wu, *Senior Member, IEEE*

***Abstract*— Model-based rotor position/speed estimators are commonly used for sensorless control of interior permanent-magnet synchronous machines (IPMSMs) operating in the medium- and high-speed regions. A rotor position/speed estimation scheme usually contains three major parts: 1) a state observer; 2) a position estimator; and 3) a speed estimator. This paper proposes a sliding-mode observer (SMO) as the state observer to estimate the position-related system states, which are the extended electromotive force components in this paper. Then, two major contributions are made to achieve improved position and speed estimation. First, the rotor speed is estimated independently using a model reference adaptive system (MRAS)-based method, which is decoupled from the position estimation. To reduce the noise contents in the estimated speed, an adaptive line enhancer is proposed to work with the SMO, leading to an improved reference model for the speed estimation. The proposed MRAS-based speed estimator has two operating modes, which are suitable for generator and motor applications, respectively. Second, the estimated rotor speed is used as a feedback input signal to mitigate the oscillating error in the estimated rotor position, leading to an integrated position and speed estimation system. The effectiveness of the proposed position and speed estimators is verified by simulation using the data logged from a real-world test vehicle. Experimental results on a test stand of an IPMSM drive system used in off-road, heavy-duty hybrid electric vehicles are also provided to further validate the proposed rotor position/speed estimation schemes.**

***Index Terms*— Interior permanent-magnet synchronous machine (IPMSM), model reference adaptive system (MRAS), position/speed estimation, sensorless control.**

I. Introduction

INTERIOR permanent-magnet synchronous machines (IPMSMs) are widely used in electric and hybrid electric vehicle systems owing to their distinctive advantages, such as high efficiency, high-power density, and wide constant power region. To achieve high-performance vector control for IPMSMs, accurate rotor position information is indispensable, which, in conventional IPMSM drive systems, is usually obtained using rotary encoders or resolvers. This increases the cost, size, and wiring complexity and reduces the mechanical robustness and reliability of the IPMSM drive systems. To solve these problems, much research effort has gone into the development of rotor position/speed sensorless drives that have comparable dynamic performance to sensor-based drives during the last decades [1].

In the medium- and high-speed regions of sensorless IPMSM drive systems, the rotor position and speed are commonly estimated by model-based methods using sensed machine currents and sensed or commanded machine terminal voltages [2]–[8]. There are three major parts in those model-based position/speed estimation schemes: 1) a state observer to estimate the position/speed related system states, e.g., extended electromotive force (EEMF) [5]; 2) a position estimator to extract the rotor position information from the estimated states or rotor speed; and 3) a speed estimator to extract the rotor speed from the estimated states or rotor position. Several state observers, as shown in Fig. 1(a), have designed based on the full-order IPMSM model [2], [3] for simultaneous rotor position and speed estimation. However, these state observers are usually complicated since they were built on high-order, e.g., fourth-order, IPMSM models. In addition, it is difficult to guarantee the convergence of both speed and position estimation simultaneously under fast varying speed/torque conditions. To simplify the observation algorithm and improve the dynamic state tracking performance, several state observers, such as disturbance observers [4], [5] and sliding-mode observers (SMOs) [6], [7], have been designed to effectively estimate the position/speed related system states based on reduced-order, such as the second-order, IPMSM models in sensorless IPMSM drive systems. From the estimated states either rotor position or speed can be obtained. Then, the other one can be calculated according to the relationship between speed and position.

Two major types of state observers have been designed based on the reduced-order, e.g., second-order, IPMSM models, as shown in Fig. 1(b) and (c). The method presented in [4] was performed in the rotor reference frame, where the rotor speed was first estimated form the estimated system states and then the rotor position was obtained by integrating the

Manuscript received October 5, 2013; revised December 4, 2013; accepted January 2, 2014. Date of publication January 9, 2014; date of current version July 30, 2014. This work was supported in part by the John Deere Electronic Solutions and in part by the U.S. National Science Foundation under Grant ECCS-0901218. Recommended for publication by Associate Editor Baiming Shao.

Y. Zhao and W. Qiao are with the Power and Energy Systems Laboratory, Department of Electrical Engineering, University of Nebraska-Lincoln, Lincoln, NE 68588-0511 USA (e-mail: yue.zhao@huskers.unl.edu; wqiao@engr.unl.edu).

L. Wu is with the John Deere Electronic Solutions, Fargo, ND 58102 USA (e-mail: wulong@johndeere.com).

Color versions of one or more of the figures in this paper are available online at http://ieeexplore.ieee.org.

Digital Object Identifier 10.1109/JESTPE.2014.2298433

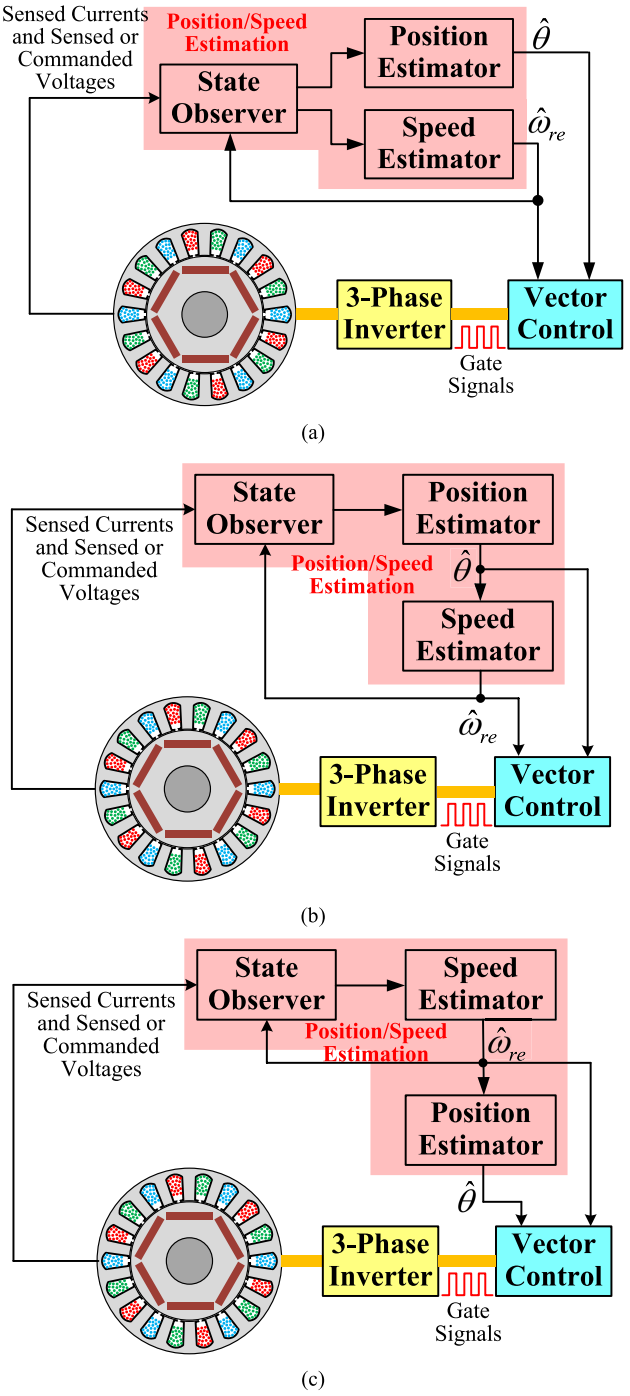

Fig. 1. Illustrations of different types of rotor position/speed estimation methods. (a) Parallel structure with position and speed estimated simultaneously and series structure with (b) position estimated first and (c) speed estimated first.

estimated rotor speed. In contrast, the methods presented in [5]–[8], were performed in the stationary reference frame, where the rotor position was extracted directly from the estimated system states using an arctangent, phase-locked loop (PLL), or Luenberger observer. The rotor speed can then be obtained from the estimated rotor position. In practical applications, due to the cascaded structure, the performance of the position and speed estimators may not be acceptable during large load and machine parameter variations. For example, there are several inherent drawbacks in the position/speed estimation method in Fig. 1(b). First of all, since the position estimator and the speed estimator are connected sequentially without a feedback or other adjustment schemes, any error will propagate in the loop. For instance, if the state observer has improper gains, the performance of the following position and speed estimators will be affected. Since the speed estimator is the last module in the loop, it will be affected by the performance of all the subsystems prior to it. Second, the position estimation is sensitive to load variations. Since the speed is calculated from the estimated position, the speed estimation is also sensitive to load variations.

An effective solution to the problems of the estimators shown in Fig. 1(b) and (c) is to decouple the rotor speed and position estimation, i.e., estimating speed and position independently. In this paper, an SMO [7] is designed to estimate the EEMF of an IPMSM. Based on the estimated EEMF, the rotor position and speed are estimated separately. A model reference adaptive system (MRAS)-based speed estimator [9] is proposed to estimate the rotor speed using a heterodyning speed adaption mechanism. An adaptive line enhancer (ALE) is proposed to filter the estimated EEMF without introducing any phase delay between the original and filtered EEMF components. Compared with the case without the ALE, the SMO plus the ALE provides an improved reference model in the MARS. The proposed MRAS speed estimator has two different operating modes, which can be utilized for different IPMSM applications in vehicles, such as traction motors and generators.

Among different state observers used in the model-based sensorless control schemes, the SMO is a promising candidate due to the feature of high robustness to system structure and parameter uncertainties. In particular, the sliding-mode technique is becoming more and more attractive due to the widespread use of digital control systems over the last two decades. The conventional sliding-mode technique [10] requires a high-sampling frequency to ensure the proper operation of the observer. In a discrete-time SMO, to facilitate digital implementation, the observer input is calculated once per sampling period and is held constant during this interval. Due to the limited sampling frequency, the trajectory of the state of interest is unable to exactly move along the sliding surface, leading to a quasisliding-mode motion [11], [12]. In the previous work of the SMO-based sensorless PMSM drives [6]–[8], a high-sampling frequency is always required. Without oversampling, the performance of the SMO will be poor and unacceptable [13].

In industrial applications, such as generators in electric vehicles, considering switching losses as well as thermal and electromagnetic interference (EMI) issues, the switching frequency of the rectifiers/inverters is usually selected such that there are 10–20 switching cycles per electric revolution. In the vector control, the phase currents are usually sensed once per switching cycle. When using the sensed currents for position/speed estimation, the low-sampling ratio of the phase current will pose challenges to the application of a discrete-time SMO, where the sampling ratio is defined to be the number of current samples per electric revolution. As a result, the waveforms of the estimated EEMF components will have distortions,

which will include both phase shift and magnitude variation. In this case, conventional position estimators, e.g., the PLL, will suffer an oscillation problem when extracting the position information from the distorted EEMF components. The estimated rotor position will have large noise and errors.

To further improve the quality of position estimation, this paper proposes a novel estimated rotor speed feedback-based oscillation mitigation scheme [14]. This scheme has a filtering effect on the estimated position to mitigate the position oscillation caused using a low-sampling ratio. The proposed MRAS-based rotor speed estimator and the SMO-based rotor position estimator with the oscillation mitigation algorithm lead to an integrated position/speed estimation system with improved estimation performance for sensorless control of IPMSMs. The effectiveness of the proposed rotor position and speed estimators is verified by simulation studies using real-world data logged from a test hybrid electric vehicle. Experimental results obtained from a test stand of an IPMSM drive system used in off-road, heavy-duty hybrid electric vehicles are also provided to further validate the proposed rotor position and speed estimators.

II. Conventional MRAS-Based Rotor Speed Estimator for IPMSMs

The MRAS [15]–[22] is an effective scheme for speed estimation in different motor drives, e.g., PMSMs [21], [22], induction motors [15]–[19], and brushless dc motors [20]. In a MRAS, an adjustable model and a reference model are connected in parallel. The structure of a typical MRAS-based speed estimator is shown in Fig. 2. In this paper, the EEMF is estimated using an SMO [7], which contains the information of the rotor speed and is a good candidate for the reference model. Then, an adjustable model should be designed to output the EEMF as well while using the rotor speed as an internal state, whose value is updated (estimated) by an adaptive mechanism. With a proper adaptive mechanism, the output of the adjustable model is expected to converge to the output of the reference model. In this case, the internal states of the two models should be identical. Thus, the rotor speed estimated by the adaptive mechanism will converge to the actual rotor speed contained in the reference model. From this point of view the adjustable model is a kind of adaptive filter/observer.

The design of the adjustable model is originated from the EEMF model of an IPMSM, which can be expressed as

$$\begin{bmatrix} v_\alpha \\ v_\beta \end{bmatrix} = \begin{bmatrix} R + pL_d & \omega_{re}(L_d - L_q) \\ \omega_{re}(L_q - L_d) & R + pL_d \end{bmatrix} \begin{bmatrix} i_\alpha \\ i_\beta \end{bmatrix} + \begin{bmatrix} E_\alpha \\ E_\beta \end{bmatrix} \quad (1)$$

where p is the derivative operator; v_α and v_β are the stator voltage components defined in the $\alpha\beta$ stationary reference frame; i_α and i_β are the stator current components defined in the $\alpha\beta$ stationary reference frame; ω_{re} is the electrical rotor speed; R is the stator resistance; and L_d and L_q are the d-axis and q-axis inductances in the rotor reference frame, respectively; and the EEMF components $E_{\alpha\beta} = [E_\alpha,\ E_\beta]^T$ are defined as

$$\begin{bmatrix} E_\alpha \\ E_\beta \end{bmatrix} = \left[(L_d - L_q)(\omega_{re} i_d - p i_q) + \omega_{re}\psi_m\right] \begin{bmatrix} -\sin\theta \\ \cos\theta \end{bmatrix}. \quad (2)$$

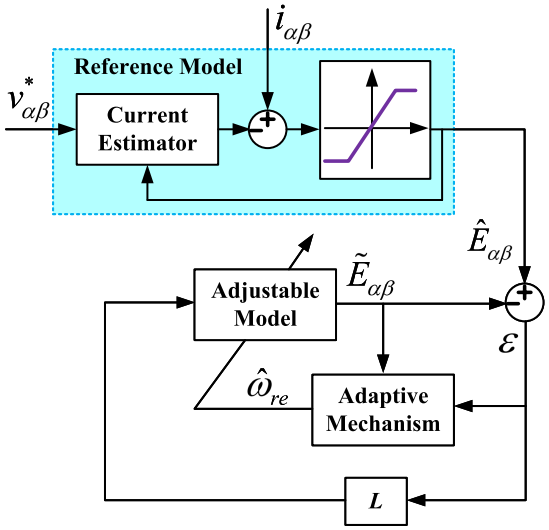

Fig. 2. Schematic of the conventional MRAS-based rotor speed estimator.

Using a properly designed SMO, the estimated EEMF components, $\hat{E}_{\alpha\beta} = [\hat{E}_\alpha,\ \hat{E}_\beta]^T$, can be obtained. If the rotor speed changes slowly, i.e., $d\omega_{re}/dt \approx 0$, which is true when the IPMSM operates in the medium- and high-speed regions, the derivatives of the estimated EEMF components can be calculated as

$$\begin{cases} \dot{\hat{E}}_\alpha = -\omega_{re}\hat{E}_\beta \\ \dot{\hat{E}}_\beta = \omega_{re}\hat{E}_\alpha. \end{cases} \quad (3)$$

The adjustable model can be designed by following the form of (3) as follows:

$$\begin{bmatrix} \dot{\tilde{E}}_\alpha \\ \dot{\tilde{E}}_\beta \end{bmatrix} = \hat{\omega}_{re} \underbrace{\begin{bmatrix} 0 & -1 \\ 1 & 0 \end{bmatrix}}_{J} \cdot \begin{bmatrix} \tilde{E}_\alpha \\ \tilde{E}_\beta \end{bmatrix} + \underbrace{\begin{bmatrix} L_{11} & L_{12} \\ L_{21} & L_{22} \end{bmatrix}}_{\mathbf{L}} \cdot \begin{bmatrix} \hat{E}_\alpha - \tilde{E}_\alpha \\ \hat{E}_\beta - \tilde{E}_\beta \end{bmatrix} \quad (4)$$

where $\tilde{E}_{\alpha\beta} = [\tilde{E}_\alpha,\ \tilde{E}_\beta]^T$ is the output vector of the adjustable model, which is also a vector of estimated EEMF components; $\hat{\omega}_{re}$ is the estimated electrical rotor speed, which is the output of the adaptive mechanism; $\mathbf{L}$ is the MRAS gain matrix, which can be configured using a linear observer design technique, e.g., pole assignment [20]. In practical applications, the off-diagonal elements, L_{21} and L_{12}, can be set to be zero [20] to simplify the design procedure. Based on the outputs of the adjustable model and the reference model, the rotor speed can be estimated using a proportional–integral (PI) speed regulator as follows:

$$\hat{\omega}_{re} = \left(k_p + \frac{k_i}{s}\right)\left[\left(\hat{E}_{\alpha\beta} - \tilde{E}_{\alpha\beta}\right)^T \cdot J \cdot \tilde{E}_{\alpha\beta}\right]. \quad (5)$$

III. Proposed MRAS-Based Rotor Speed Estimator

In the previous section, the conventional MRAS-based rotor speed estimator using an SMO as the reference model has been discussed. However, in a practical IPMSM drive system, the SMO may not be an effective reference model due to several reasons. First, the inherent nonlinearity of the switching function, e.g., the sign function or saturation function, used in

the SMO will bring heavily noisy contents into the output of the SMO. Second, the EEMF of an IPMSM is both torque- and speed-dependent. Rewrite the expression of the EEMF defined in (2) in the following form:

$$\begin{bmatrix} E_\alpha(t) \\ E_\beta(t) \end{bmatrix} = \eta(t) \cdot \begin{bmatrix} -\sin[\omega_{re}(t) \cdot t + \theta_0] \\ \cos[\omega_{re}(t) \cdot t + \theta_0] \end{bmatrix} \tag{6}$$

where θ_0 is the initial rotor position. The magnitude of the EEMF, $\eta(t)$, is time-variant and depends on the magnitudes of both currents and rotor speed. Under fast varying load conditions, the current derivative term, pi_q, could be a large and varying component, which results in a larger variation in $\eta(t)$. In addition, when the torque is not constant, the rotor speed, ω_{re}, will have an oscillation due to imperfect rotor speed regulation. Considering these issues, an ALE is designed to effectively filter out the noisy contents from the estimated EEMF components. The resulting SMO with the ALE provides an improved reference model for the MRAS. In addition, a heterodyning speed adaption mechanism is proposed to replace the adaptive mechanism (5). Compared with (5), the proposed heterodyning speed adaption mechanism has the following advantages: 1) it has a lower computational cost and 2) it is easier to design its PI gains because it only relies on the normalized values of the estimated EEMF components.

A. Adaptive Line Enhancer

Consider a noisy signal, which consists of a few desired sinusoidal components. When the frequencies of the sinusoidal components in the noisy signal are known, a fixed filter will be sufficient to extract the sinusoidal components. However, when the sinusoidal frequencies of the noisy signal, e.g., the EEMF components in (6), are unknown or time-varying, an adaptive filter will be required. The ALE [23] is a good candidate of such an adaptive filter. Consider that a noisy input signal $x(n)$ of the ALE contains X sinusoidal components and can be modeled as follows:

$$x(n) = \sum_{i=1}^{X} a_i \sin[\omega_i n + \theta_i] + v(n) \tag{7}$$

where ω_i, a_i and θ_i are the frequency, amplitude, and phase angle of the ith sinusoidal component, and $v(n)$ is the noise, which may not be white. Suppose that any two samples of the noise term which are more than M sampling intervals apart are uncorrelated with each other. In this case, the ALE is an M-step-ahead predictor. Fig. 3 depicts the block diagram of the ALE, which predicts the sinusoidal components in $x(n)$, while filtering out the noise component. When the filter $W(z)$ is adapted to minimize the mean-square error between the output and input signals, the ALE will be a filter tuned to only extract the sinusoidal components. The output of the filter, $y(n)$, will be an approximation of the sum of the sinusoidal components. Consider (6) again, if the currents and rotor speed are time-variant, the EEMF components can be modeled as the sums of all the sinusoidal components

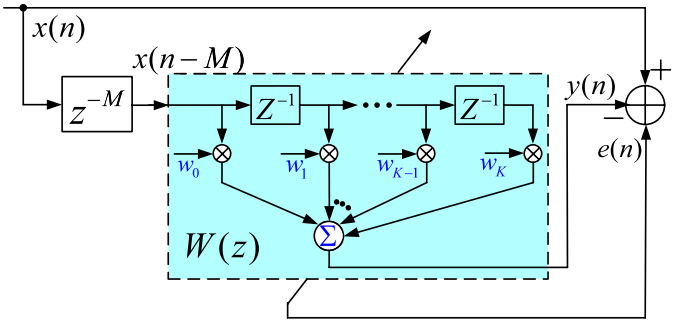

Fig. 3. Block diagram of the ALE.

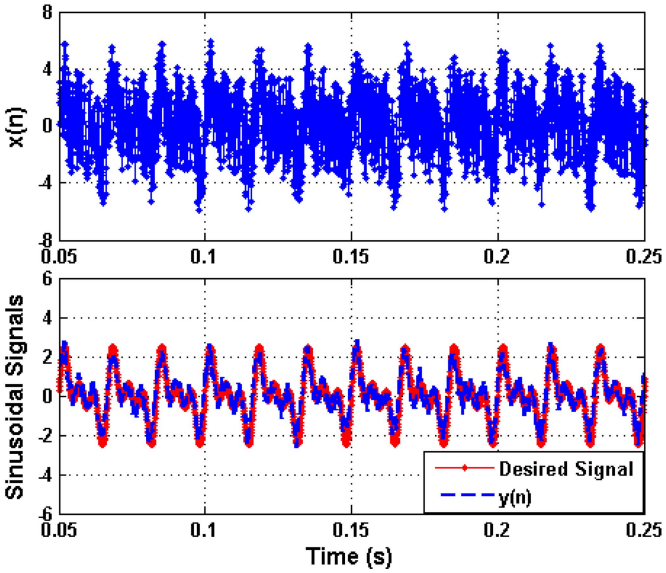

Fig. 4. Simulation result of the filtering performance of the ALE for an artificial data input.

with different frequencies as follows:

$$\begin{bmatrix} E_\alpha(t) \\ E_\beta(t) \end{bmatrix} = \sum_{i=1}^{H} \begin{Bmatrix} -a_i \sin[\omega_i t + \theta_i(t)] + v_i(t) \\ a_i \cos[\omega_i t + \theta_i(t)] + v_i(t) \end{Bmatrix} \tag{8}$$

where ω_i, a_i and $\theta_i(t)$ are the frequency, amplitude, and time-varying phase angle of the ith component; $v_i(t)$ is the corresponding noise; and H is the number of the sinusoidal components. The number of the filter taps, K, in Fig. 3 should be greater than H, and the tap weight matrix, $\mathbf{w} = [w_0, w_1, \ldots, w_K]$, can be calculated online using the well known least-mean-square algorithm

$$\mathbf{w}(n+1) = \mathbf{w}(n) + 2\mu e(n) x(n) \tag{9}$$

where μ is the step size for $\mathbf{w}$ adaption.

The simulation result for a simple case study is shown in Fig. 4. The desired signal consists of three sinusoidal components with the frequencies of 60, 120, and 180 Hz, respectively. The power of the noise is equal to that of the desired signal. The sampling frequency is 6 kHz. As the result shows, the ALE effectively filters out the noise contents without any phase shift or magnitude decrease. The output of the ALE converges to the desired signal within 30 samples.

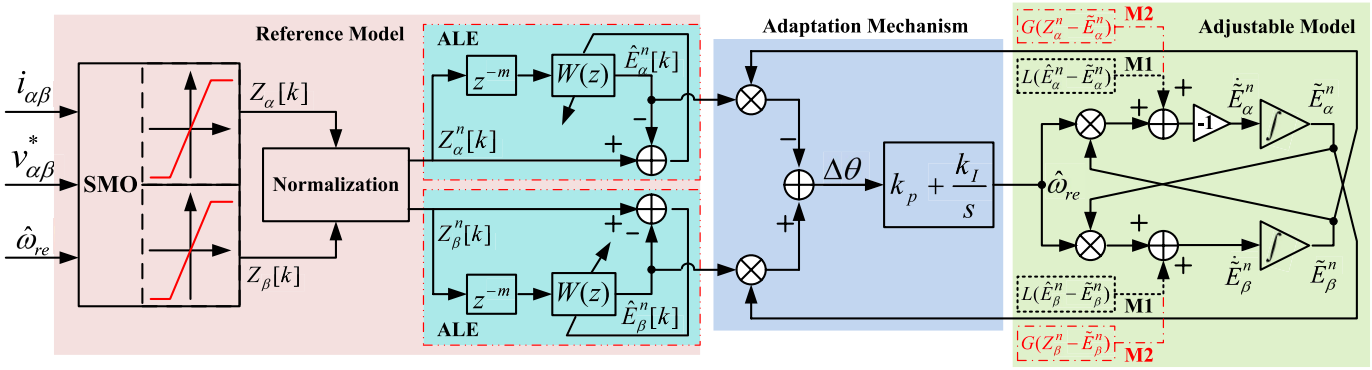

Fig. 5. Schematic diagram of the proposed MRAS-based rotor speed estimator.

B. Heterodyning Speed Adaption Mechanism

In addition to the ALE, a heterodyning speed adaption mechanism is designed to replace (5). Based on the two estimated EEMF vectors, $\hat{E}_{\alpha\beta}$ and $\tilde{E}_{\alpha\beta}$, in the MRAS, the heterodyning speed adaption scheme can be expressed as

$$\hat{\omega}_{re} = \left(k_p + \frac{k_i}{s}\right)\left(\hat{E}^n_\beta \tilde{E}^n_\alpha - \hat{E}^n_\alpha \tilde{E}^n_\beta\right) \tag{10}$$

where the superscript n stands for the normalized values of the quantities with respect to their amplitudes. Let $\hat{\theta}$ and $\tilde{\theta}$ represent the rotor positions obtained from $\hat{E}_{\alpha\beta}$ and $\tilde{E}_{\alpha\beta}$, respectively, and define

$$\hat{E}^n_{\alpha\beta} = \left[-\sin\hat{\theta}\ \cos\hat{\theta}\right]^T \quad \text{and} \quad \tilde{E}^n_{\alpha\beta} = \left[-\sin\tilde{\theta}\ \cos\tilde{\theta}\right]^T. \tag{11}$$

Substituting (11) into (10) yields

$$\begin{aligned}\hat{\omega}_{re} &= s\tilde{\theta} = \left(k_p + \frac{k_i}{s}\right)\left(-\cos\hat{\theta}\sin\tilde{\theta} + \sin\hat{\theta}\cos\tilde{\theta}\right) \\ &= \left(k_p + \frac{k_i}{s}\right)\sin\left(\hat{\theta} - \tilde{\theta}\right) \overset{\Delta\theta=\hat{\theta}-\tilde{\theta}\approx 0}{\longrightarrow} \approx \left(k_p + \frac{k_i}{s}\right)\Delta\theta. \end{aligned} \tag{12}$$

Then the transfer function can be expressed as

$$\frac{\tilde{\theta}}{\hat{\theta}} = \frac{k_p s + k_i}{s^2 + k_p s + k_i}. \tag{13}$$

Equation (13) represents a second-order system which has one zero. The dynamic behavior of (13) depends on the PI gains, which can be determined by properly placing the poles of the characteristic polynomial of the transfer function.

Compared with the conventional speed adaption mechanism (5), the proposed scheme (10) consumes less computational time and is easier for digital system implementation. In addition, since (10) relies on the normalized values of the estimated EEMF components, whose amplitudes are limited within $[-1, 1]$, it will be easier to design the PI gains compared with that when using (5), which relies on the estimated EEMF components with varying amplitudes.

C. Overall Rotor Speed Estimator

The overall schematic diagram of the proposed rotor speed estimator, including the SMO proposed in [7], the ALE, the heterodyning speed adaption mechanism, and the adjustable model, is shown in Fig. 5. A proof of the stability of the proposed speed estimator using Popov's hyperstability criterion is provided in the Appendix. The proposed speed estimator has two operating modes, which are suitable for different applications. In Mode I (M1), the error feedback to the adjustable model is the difference between the $\hat{E}^n_{\alpha\beta}$ and $\tilde{E}^n_{\alpha\beta}$. Due to the filtering effect of the ALE, the dynamic response of speed tracking will be slightly affected. However, the estimated speed will have less noise contents, which results in a smooth speed profile. Therefore, Mode I is suitable for generator applications, in which the rotor speed of the generator is normally maintained by a prime mover machine, and the sensorless control performance is not sensitive to the estimated rotor speed.

In Mode II (M2), the error feedback to the adjustable model is the difference between $Z^n_{\alpha\beta}$ and $\tilde{E}^n_{\alpha\beta}$. Since $Z^n_{\alpha\beta}$ is the unfiltered normalized output of the SMO, sending $Z^n_{\alpha\beta}$ back to the adjustable model will force the output of the adjustable model to approach the unfiltered EEMF estimated from the SMO. This scheme does not have the misadjustment caused by the ALE during abrupt speed changes and improves the dynamic response of speed tracking. However, the estimated rotor speed will have relatively larger noise contents compared to that in Mode I, which will result in ripples in the estimated rotor speed. Mode II is suitable for motor drive applications, in which the sensorless control requires accurate rotor speed information without any delay, especially when the drive system is operated in the speed control mode.

IV. Oscillation Mitigation Scheme for Rotor Position Estimation Using Estimated Rotor Speed Feedback

A. Problem Description

Per previous discussion, in a discrete-time SMO, the reaching law will force the state trajectory moving toward the designed sliding surface. However, due to the use of a finite sampling frequency, the trajectory of the state of interest cannot exactly move along the sliding surface. As a result, the state tracking errors cannot be fully eliminated, namely, the state trajectory will have a bounded motion around the sliding surface and cause a chattering problem. The amplitude of chattering can be reduced by increasing the sampling rate, but cannot be eliminated unless the sampling period $T_s \rightarrow 0$ [10]. In a practical electric drive system, due to

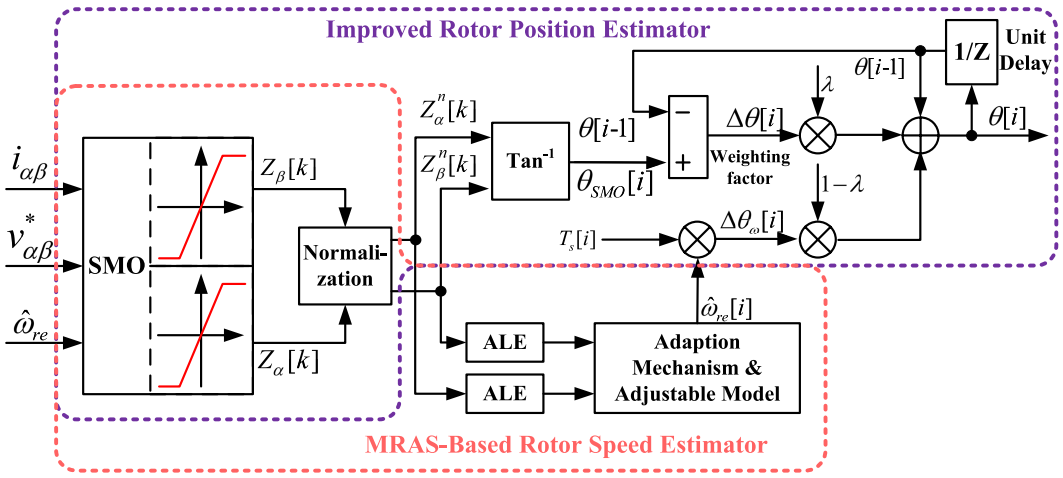

Fig. 6. Schematic of the proposed improved rotor position estimator.

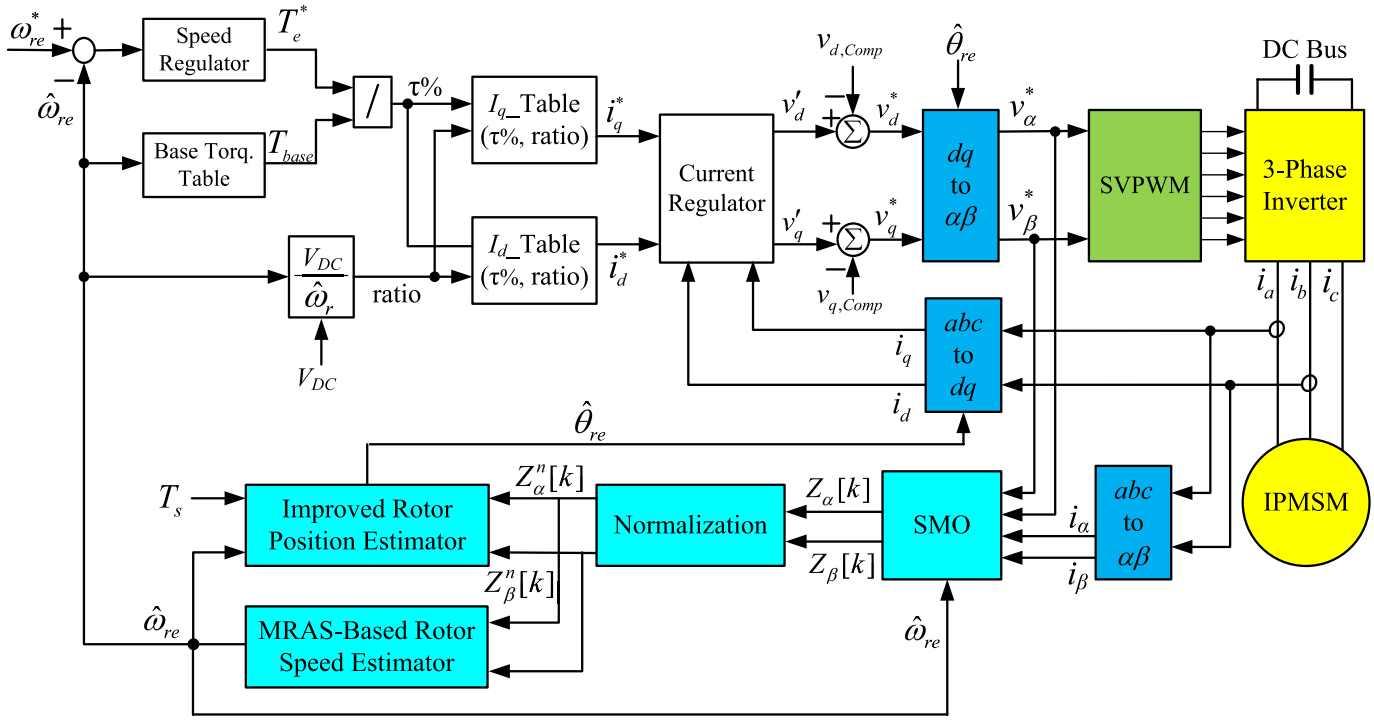

Fig. 7. Overall schematic diagram of the proposed sensorless control scheme for an IPMSM.

switching losses, EMI, and thermal issues in the inverter and limited computational resource, the sampling frequency should be selected appropriately according to the system dynamics to guarantee fast response [24], instead of for the sake of the control algorithms. When designing the rotor position estimator, if the rotor position is extracted from the estimated EEMF by an SMO which has a chattering problem, there will be an oscillating error between the actual and estimated rotor positions. An appropriate method is needed to mitigate the oscillating rotor position estimation error.

B. Oscillation Mitigation Scheme Using the Estimated Rotor Speed Feedback

As presented in Section III, the rotor speed can be estimated by the proposed MRAS-based speed estimator. Denote the estimated rotor speed in the ith sampling period as $\hat{\omega}_{re}[i]$. In the steady state, suppose that the rotor speed is maintained as a constant during one sampling period, the change in the position during the ith sampling period, $\Delta\theta_{\omega}[i]$, can be estimated as

$$\Delta\theta_{\omega}[i] = \hat{\omega}_{re}[i] \times T_s[i] \tag{14}$$

where T_s is the sampling period.

Equation (14) provides additional information on the change in the rotor position, which can be used to mitigate the oscillating problem of the rotor position obtained from the EEMF estimated by the SMO. Using the rotor speed as a feedback input signal, the rotor position can be estimated as follows:

$$\theta[i] = \theta[i-1] + \lambda \times \Delta\theta[i] + (1-\lambda) \times \Delta\theta_{\omega}[i] \tag{15}$$

TABLE I
SPECIFICATIONS OF THE IPMSM

Maximum power	155 kW	Stator resistance	0.01 Ω
Maximum torque	300 Nm	Base speed	5000 RPM
Rated Current	400 A	Pole pairs number	4
Average L_d	0.2 mH	Average L_q	0.75 mH

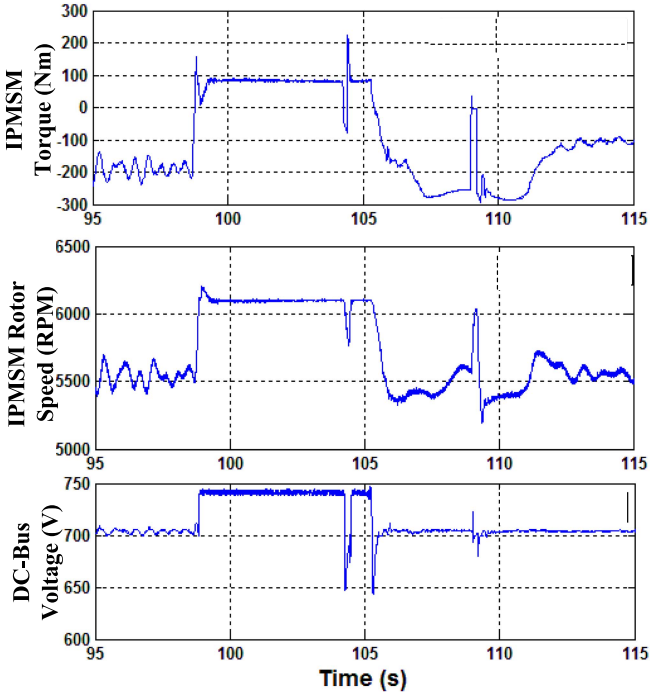

Fig. 8. Real-world vehicle data profiles used for simulation studies.

where $\theta[i]$ is the estimated rotor position in the ith sampling period; $\theta[i-1]$ is the estimated rotor position in the previous sampling period; $\Delta\theta[i] = \theta_{\text{SMO}}[i] - \theta[i-1]$, where $\theta_{\text{SMO}}[i]$ is the rotor position obtained directly from the SMO-estimated EEMF components using the arctangent operation; λ is a weighting factor used to adjust the contribution of the estimated speed in the position update. If $\lambda = 1$, then $\theta[i] = \theta_{\text{SMO}}[i]$, which means that there is no speed feedback. Otherwise, if $\lambda = 0$, the rotor position is updated using the estimated speed feedback only.

Different from the estimated rotor speed feedback-based oscillation mitigation scheme presented in [14], in which the rotor speed was calculated from the estimated position using a moving average (MA) filter, in this paper, the rotor speed is estimated using the proposed MRAS-based estimator. Since the proposed speed estimator has a better dynamic response compared with the MA filter, the oscillation mitigation performance of the method presented in this paper is better than that presented in [14]. Both simulation and experimental results will be presented later to verify this statement. Fig. 6 shows the schematic of the proposed improved rotor position estimator.

V. Overall Sensorless Control Scheme for an IPMSM Drive System

Fig. 7 shows the overall schematic diagram of the proposed sensorless control scheme for an IPMSM, where the

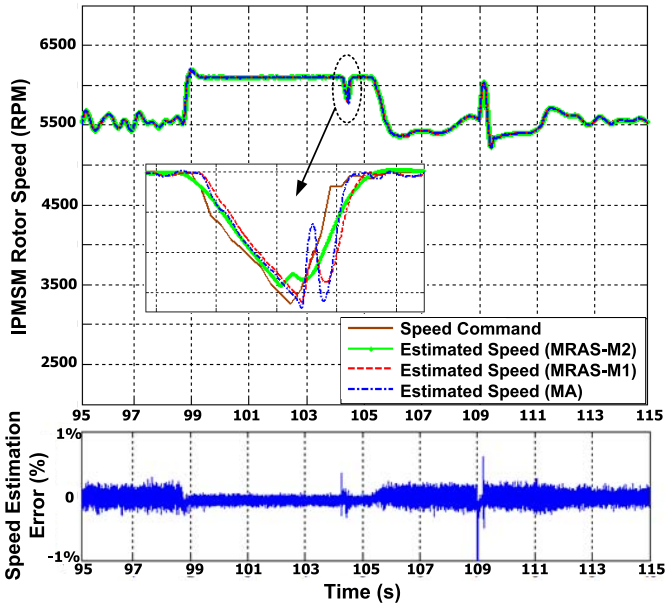

Fig. 9. Speed estimation results using the proposed speed estimator and an MA filter.

rotor position and speed are estimated using the proposed estimators. The outer loop of the control scheme is a speed PI regulator, which is used to generate the torque command based on the speed tracking error. The base torque is the maximum allowable output torque at each speed point, which is obtained from a 2-D lookup table. The torque percentage, i.e., the ratio between the commanded torque and the base torque, is used as one argument to determine the current command. Since the dc-bus voltage will affect the optimal current commands of the drive system, a voltage/speed ratio is used as the other argument to determine the current commands. The current commands are then generated by two lookup tables based on the torque percentage and voltage/speed ratio. Other modules of the drive system, including coordinate transformations, current regulators with feedforward voltage compensation, space vector pulse-width modulator, three-phase inverter, and IPMSM, are also shown in Fig. 7. The major parameters of the IPMSM used in both simulation and experiments are listed in Table I.

VI. Simulation Results

Simulation studies using the data logged from a real-world test vehicle are performed. The effectiveness of both the proposed MRAS-based rotor speed estimator and the oscillation mitigation scheme for rotor position estimation is validated by simulation results. The overall sensorless IPMSM drive system presented in Section V is implemented in MATLAB/Simulink.

A. Simulation Results of the MRAS-Based Rotor Speed Estimator

Real-world vehicle data are used for simulation studies to verify the performance of the proposed MRAS-based rotor speed estimator. The data were logged from an IPMSM

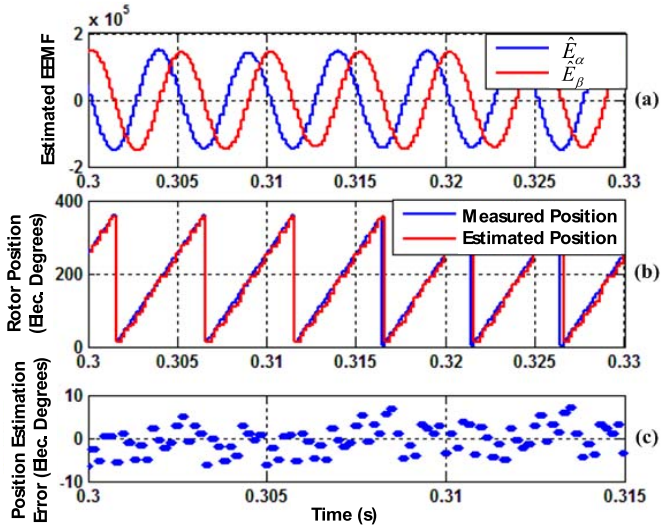

Fig. 10. Simulation results for the proposed position estimator without the oscillation mitigation scheme. (a) Estimated EEMF components. (b) Measured and estimated positions. (c) Position estimation error.

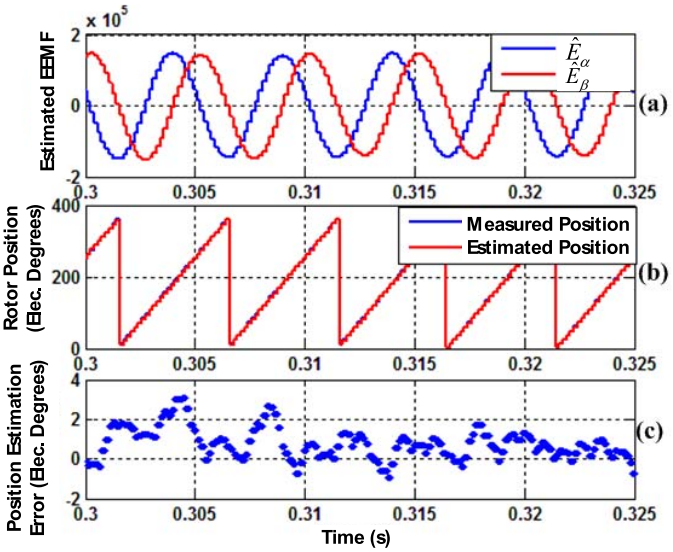

Fig. 11. Simulation results for the proposed position estimator with the oscillation mitigation scheme (when $\lambda = 0.1$). (a) Estimated EEMF components. (b) Measured and estimated positions. (c) Position estimation error.

operating as a generator on a test off-road vehicle. Fig. 8 shows the torque and speed of the IPMSM and the dc-bus voltage of the vehicle during one typical driving cycle. In the simulation, the IPMSM is operated in the torque control mode using the profile shown in Fig. 8 as the torque command. When the torque has a higher slew-rate change, e.g., around 104 s, an obvious abrupt speed dip is observed correspondingly, which is a critical period for performance evaluation of the proposed rotor speed estimator.

The corresponding simulation results of the rotor speed are shown in Fig. 9, which includes the speed command, the estimated speed obtained from the estimated rotor position using an MA filter, and the speeds obtained from the proposed

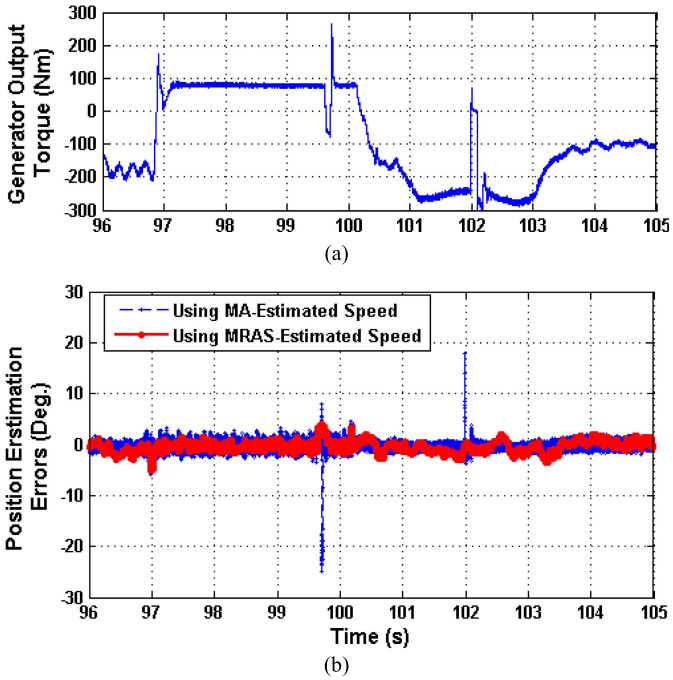

Fig. 12. Comparison of simulation results of the methods presented in this paper and in [14]. (a) Output torque profile of the IPMSM generator. (b) Position estimation errors.

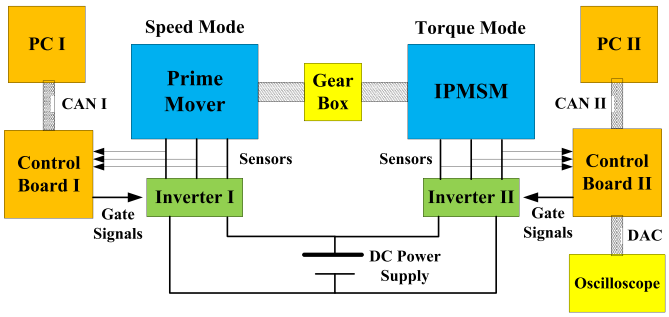

Fig. 13. Schematic of the test stand for the IPMSM.

MRAS speed estimator in both operating modes. During the large speed transient around the 104th second, the speeds estimated by the MA and the proposed MRAS in Mode I can track the desired value. However, both of the estimated speeds have obvious delays and relatively large estimation errors caused by the large load transition, where the maximum speed estimation error of MA reaches 150 r/min, i.e., 3% when using 5000 r/min as the base. Compared to the MA and the MRAS in Mode I, the delay in the speed estimation is negligible and the magnitude of the speed estimation error obtained from the MRAS in Mode II with respect to the speed command is always smaller, i.e., less than 1%.

B. Simulation Results of the Oscillation Mitigation Scheme in the Proposed Rotor Position Estimator

Simulation studies are performed to compare the performance of the proposed rotor position estimator without and with the estimated rotor speed feedback-based oscillation

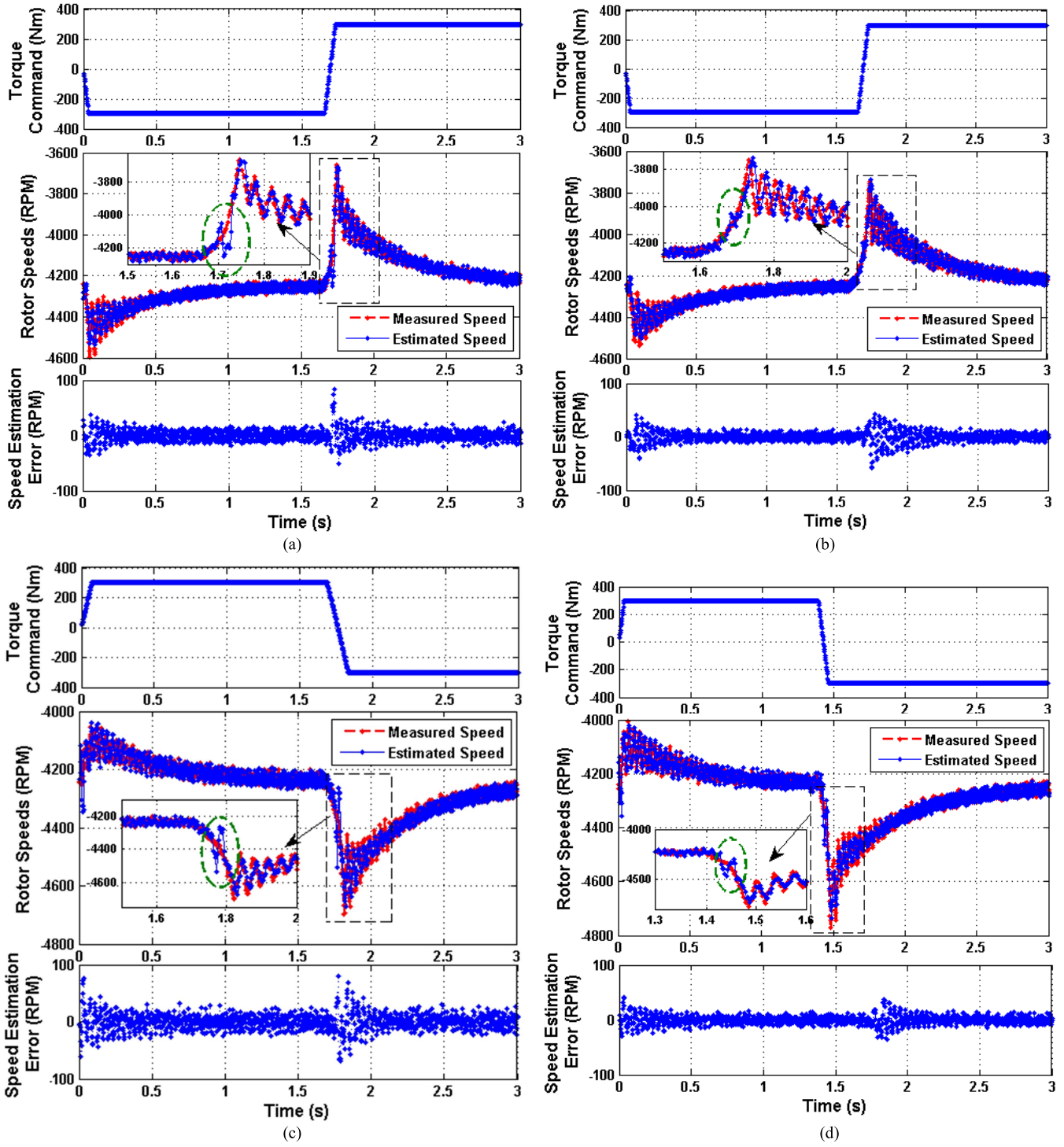

Fig. 14. Experimental results during complete torque reversals (a) from full motoring to full braking using the conventional MRAS; (b) from full motoring to full braking using the proposed MRAS in Mode II; (c) from full braking to full motoring using the conventional MRAS; and (d) from full braking to full motoring using the proposed MRAS in Mode II.

mitigation scheme, and the steady-state results are shown in Figs. 10 and 11, respectively. In the simulation, the rotor speed is 3000 r/min and the corresponding fundamental frequency of the EEMF is 200 Hz; the weight λ in (15) is selected to be 0.1. In Fig. 10, due to the noise contents in the estimated EEMF, the estimated position has many oscillations, and the position estimation error is relatively large within ± 10 electric degrees, as shown in Fig. 10(c). As Fig. 11(a) shows, the estimated EEMF is exactly the same as that in Fig. 10(a), since the oscillation mitigation algorithm only modifies the estimated position, but has no effect on the EEMF estimated by the SMO. As shown in Fig. 9, the speed estimation error is

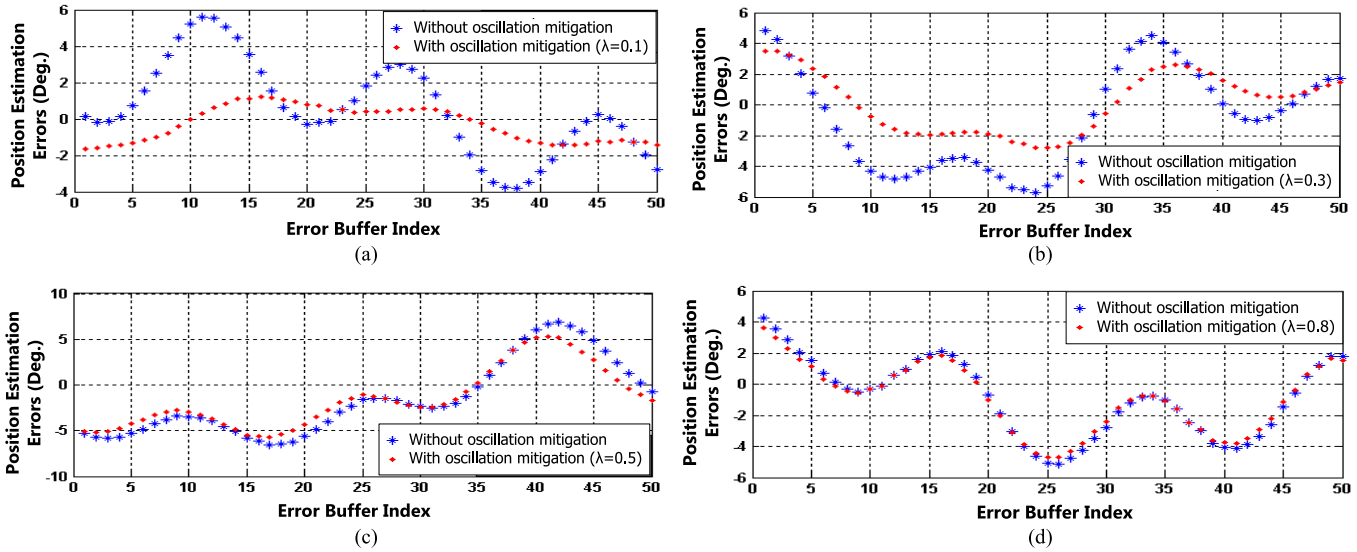

Fig. 15. Comparison of position estimation errors obtained from the proposed rotor position estimator without and with the oscillation mitigation scheme using different weight λ. (a) $\lambda = 0.1$. (b) $\lambda = 0.3$. (c) $\lambda = 0.5$. (d) $\lambda = 0.8$.

always smaller than 1%, namely, the speed estimation error is limited within ± 30 r/min when the rotor speed is 3000 r/min. Using the maximum speed estimation error of 1% of the operating speed (i.e., 30 r/min) in this simulation paper, for one sampling period, the position estimation error caused by the speed estimation error is only 0.12 electric degrees, which is so small such that has little effect on the position estimation. As shown in Fig. 11, using the proposed rotor position estimation algorithm, the estimated and measured rotor positions are on top of each other. The position estimation error is almost limited within ± 3 electric degrees. The position oscillation problem has been significantly mitigated at steady state, when compared with the position estimator without the proposed oscillation mitigation scheme.

The transient performance of the proposed oscillation mitigation scheme is also evaluated using the real-world vehicle data shown in Fig. 8. Fig. 12 compares the rotor position estimation errors obtained from the methods presented in this paper and in [14]. In this paper, the rotor speed is estimated using the proposed MRAS-based speed estimator. While in [14], the rotor speed is estimated from the estimated rotor position using an MA filter. As shown in Fig. 12(b), when the generator torque is constant or has a slow slew-rate variation, the two methods have almost identical oscillation mitigation performance. However, when the generator torque has abruptly changes, e.g., around 99.7 and 102 s, due to the delay in the estimated speed caused by the MA filter, large position estimation errors ($>$20 electric degrees) are observed when using the method presented in [14]. On the contrary, the abruptly torque changes have no effect on the position estimation error when the method presented in this paper is used.

VII. Experimental Results

A. Experimental Test Stand Description

A test stand is designed to further validate the proposed rotor position and speed estimators. In the test stand, a prime mover machine and a test IPMSM are connected back to back sharing a common 700 V dc bus, which is served by a dc power supply. The prime mover machine maintains the shaft speed while the IPMSM works as a generator in the torque control mode. The schematic of the test stand is shown in Fig. 13. The specifications of the test IPMSM are listed in Table I.

B. Performance Evaluation for the Proposed MRAS Rotor Speed Estimator

Complete torque reversals, i.e., reversing the torque from the rated motoring torque to the rated braking toque and vice versa, are used to mimic a large load transient in Fig. 8. The performance of the conventional MRAS and the proposed MRAS in Mode II in the complete torque reversal tests is compared in Fig. 14. Because of the fast torque reversals, the rotor speed has sudden changes, e.g., around 500 r/min drop in Fig. 14(a) and (b) and 500 r/min increase in Fig. 14(c) and (d). Both the conventional MRAS and the proposed MRAS in Mode II can track the speed changes. However, the speed estimated form the conventional MRAS has an unwanted large oscillation as highlighted in the dashed-line circles in Fig. 14(a) and (c). On the other hand, no obvious unwanted oscillation is observed in the speed estimated from the proposed MRAS in Mode II. Using 5000 r/min as the speed base, the speed estimation error of the proposed MRAS in Mode II is always smaller than 1% in steady state and during large load transient; while the speed estimation error is nearly 2% during large load transient when using the conventional MRAS.

C. Performance Evaluation for the Proposed Rotor Position Estimator

Fig. 15 compares the position estimation errors obtained from the proposed rotor position estimator without and with the oscillation mitigation scheme using different weight λ.

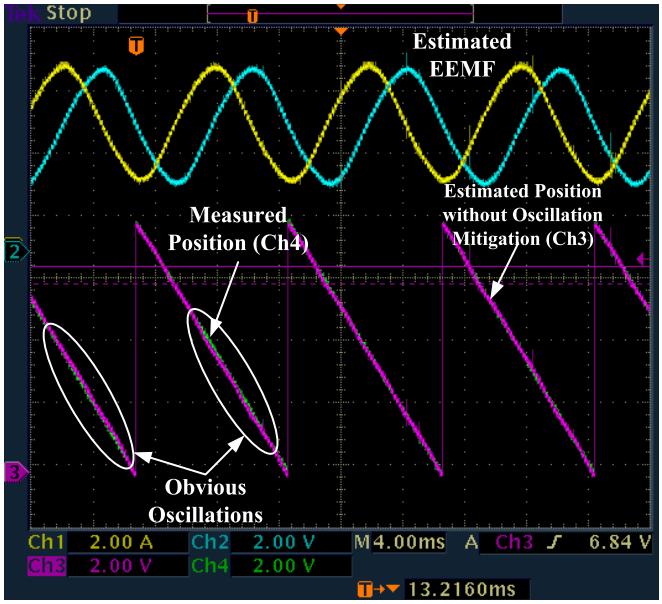

Fig. 16. Experimental results when using the proposed rotor position estimator without the oscillation mitigation scheme, where the rotor speed is 1500 r/min.

Fig. 17. Comparison of the measured and estimated rotor positions for $\lambda = 0.1$ when the rotor speed is 1500 r/min.

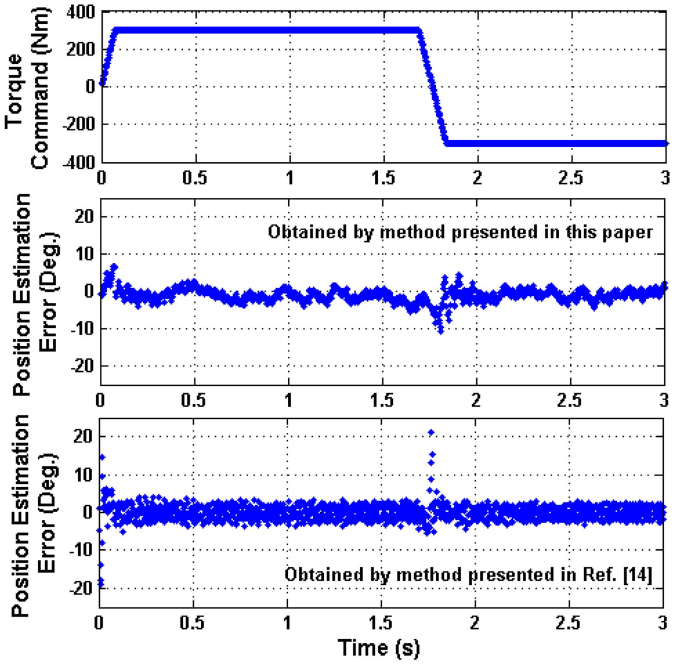

Fig. 18. Comparison of transient performance of the methods proposed in this paper and in [14] under a complete torque reversal from full braking to full motoring.

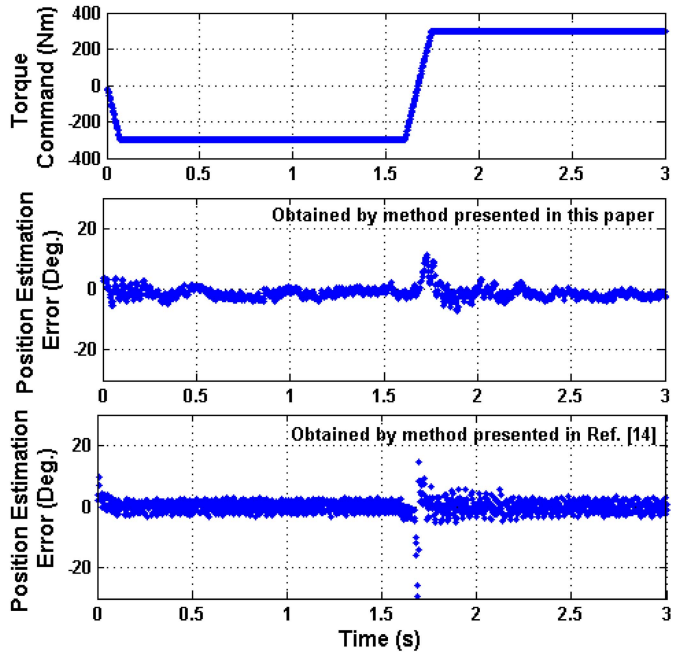

Fig. 19. Comparison of transient performance of the methods proposed in this paper and in [14] under a complete torque reversal from full motoring to full braking.

In all of the tests, the rotor speed is 3000 r/min and the sampling frequency of current measurements is 6 kHz. The effect of the rotor speed feedback on the rotor position estimation reduces with the increase of λ. When λ is larger than 0.8, the speed feedback has little effect on the estimated position. Even when λ decreases to 0.5, it is not obvious to observe the position filtering effect. However, when λ further decreases to 0.3 and 0.1, the magnitude of oscillation of the position estimation error is reduced significantly, and the variance of the oscillation becomes closer to zero. As Fig. 15(a) shows, when $\lambda = 0.1$, the position estimation error is limited within ± 2 electric degrees, which agrees with the simulation result presented in Fig. 11.

Fig. 16 shows the experimental results when using the proposed position estimator without the oscillation mitigation scheme, where the rotor speed is 1500 r/min. The curves of the measured and estimated rotor positions are on top of each other. However, it is still obvious to observe that the estimated position has small oscillations. As a

comparison, the estimated rotor position obtained from the proposed position estimator with the oscillation mitigation scheme is shown in Fig. 17, where $\lambda = 0.1$. It can be seen that the oscillation in the estimated rotor position has been effectively mitigated.

The transient performance of the rotor position estimation methods proposed in this paper and in [14] during complete torque reversals is compared in Figs. 18 and 19. When the torque command has fast slew-rate changes during the complete torque reversals, the position estimation error of the method presented in [14] has large spikes, whose magnitudes exceed 20 electric degrees. As a comparison, the spikes in the position estimation error during the fast torque transient are significantly mitigated using the method proposed in this paper. The results presented in Figs. 18 and 19 are coincident with the simulation results presented in Fig. 12.

VIII. Conclusion

A robust MRAS-based rotor speed estimator using a heterodyning speed adaption mechanism has been proposed for sensorless IPMSM drives. The MRAS contains an improved reference model, which uses an ALE to provide a better noise cancellation capability for the EEMF estimated from an SMO. The proposed rotor speed estimator has two operating modes, which are suitable for generator and motor applications, respectively. Furthermore, a novel oscillation mitigation algorithm using the estimated rotor speed as a feedback input signal has been proposed to work with the conventional inverse tangent method for rotor position estimation. This algorithm can mitigate the oscillations in the estimated rotor position caused by the noisy contents in the estimated EEMF. Simulation and experimental results on a 155-kW IPMSM drive system have been provided to validate the performance of proposed position and speed estimators and evaluate the effects of key parameters on the performance of the proposed estimators. The implementation of the proposed method is simple, and has low-computational cost and, therefore, has great potential for industrial applications.

Appendix

A brief proof of the stability and convergence of the proposed MRAS-based speed estimator is provided. According to (3), (4), and (11), the following relations can be obtained: $\dot{\hat{E}}^n_{\alpha\beta} = \omega_{re} J \cdot \hat{E}^n_{\alpha\beta}$ and $\dot{\tilde{E}}^n_{\alpha\beta} = \hat{\omega}_{re} J \cdot \tilde{E}^n_{\alpha\beta} + L \cdot \left(\hat{E}^n_{\alpha\beta} - \tilde{E}^n_{\alpha\beta}\right)$. Then differential equation of the EEMF tracking error is defined and examined as follows:

$$\dot{\varepsilon}^n_{\alpha\beta} = \dot{\hat{E}}^n_{\alpha\beta} - \dot{\tilde{E}}^n_{\alpha\beta} = \underbrace{(\omega_{re} J - L)}_{A} \cdot \varepsilon^n_{\alpha\beta} - \underbrace{\left(\hat{\omega}_{re} - \omega_{re}\right) J \cdot \tilde{E}^n_{\alpha\beta}}_{W}. \tag{A-1}$$

To guarantee the stability of the MRAS, the following two Popov's hyperstability criteria [15] should be satisfied simultaneously: 1) The forward path transfer matrix $(sI - A)^{-1}$ is strictly positive real. This can be theoretically verified and the verification process is the same as that in [20], which will not be repeated in this paper. 2) $\int_0^{t_0} \left[\left(\varepsilon^n_{\alpha\beta}\right)^T \cdot W\right] dt \geq -\gamma^2$ for all $t_0 \geq 0$, where γ^2 is a positive real constant. When the heterodyning speed adaption scheme (10) is chosen, a brief proof of the second criterion is

$$\begin{aligned}\int_0^{t_0} \left[\left(\varepsilon^n_{\alpha\beta}\right)^T \cdot W\right] dt &= \int_0^{t_0} \left\{\left(\varepsilon^n_{\alpha\beta}\right)^T \cdot J \cdot \tilde{E}^n_{\alpha\beta} \left(\hat{\omega}_{re} - \omega_{re}\right)\right\} dt \\ &= \int_0^{t_0} \left\{\left(\hat{E}^n_{\beta} \tilde{E}^n_{\alpha} - \hat{E}^n_{\alpha} \tilde{E}^n_{\beta}\right)\left(\hat{\omega}_{re} - \omega_{re}\right)\right\} dt.\end{aligned} \tag{A-2}$$

Substituting (10) into (A-2) yields

$$\begin{aligned}&\int_0^{t_0} \left[\left(\varepsilon^n_{\alpha\beta}\right)^T \cdot W\right] dt \\ &= \int_0^{t_0} \left\{\left(\hat{E}^n_{\beta} \tilde{E}^n_{\alpha} - \hat{E}^n_{\alpha} \tilde{E}^n_{\beta}\right)\left[\left(k_p + \frac{k_i}{s}\right)\left(\hat{E}^n_{\beta} \tilde{E}^n_{\alpha} - \hat{E}^n_{\alpha} \tilde{E}^n_{\beta}\right) - \omega_{re}\right]\right\} dt \\ &= \underbrace{k_p \int_0^{t_0} \left(\hat{E}^n_{\beta} \tilde{E}^n_{\alpha} - \hat{E}^n_{\alpha} \tilde{E}^n_{\beta}\right)^2 dt}_{I} \\ &\quad + \underbrace{\int_0^{t_0} \left\{\left(\hat{E}^n_{\beta} \tilde{E}^n_{\alpha} - \hat{E}^n_{\alpha} \tilde{E}^n_{\beta}\right)\left[k_i \int \left(\hat{E}^n_{\beta} \tilde{E}^n_{\alpha} - \hat{E}^n_{\alpha} \tilde{E}^n_{\beta}\right) d\tau - \omega_{re}\right]\right\} dt}_{II}\end{aligned} \tag{A-3}$$

where the first term I is nonnegative. For the second term II, denote

$$f(t) = k_i \int \left(\hat{E}^n_{\beta} \tilde{E}^n_{\alpha} - \hat{E}^n_{\alpha} \tilde{E}^n_{\beta}\right) d\tau - \omega_{re}$$

such that

$$\frac{d[f(t)]}{dt} = k_i \left(\hat{E}^n_{\beta} \tilde{E}^n_{\alpha} - \hat{E}^n_{\alpha} \tilde{E}^n_{\beta}\right).$$

Then

$$\begin{aligned}II &= \int_0^{t_0} \left\{\frac{1}{k_i} \frac{d[f(t)]}{dt} f(t)\right\} dt \\ &= \frac{1}{2k_i}\left[f^2(t_0) - f^2(0)\right] \geq -\frac{1}{2k_i} f^2(0).\end{aligned}$$

Thus

$$\begin{aligned}\int_0^{t_0} \left[\left(\varepsilon^n_{\alpha\beta}\right)^T \cdot W\right] dt &= I + II \geq 0 - \frac{1}{2k_i} f^2(0) \\ &= -\frac{1}{2k_i} f^2(0).\end{aligned}$$

Define $\gamma^2 = 1/2k_i f^2(0)$, which is a positive real constant. Therefore, the second criterion is satisfied.

References

[1] M. Pacas, "Sensorless drives in industrial applications," *IEEE Ind. Electron. Mag.*, vol. 5, no. 2, pp. 16–23, Jun. 2011.

[2] S. Po-ngam and S. Sangwongwanich, "Stability and dynamic performance improvement of adaptive full-order observers for sensorless PMSM drive," *IEEE Trans. Power Electron.*, vol. 27, no. 2, pp. 588–600, Feb. 2012.

[3] Z. Xu and M. F. Rahman, "An adaptive sliding stator flux observer for a direct-torque-controlled IPM synchronous motor drive," *IEEE Trans. Ind. Electron.*, vol. 54, no. 5, pp. 2398–2406, Oct. 2007.

[4] S. Morimoto, K. Kawamoto, M. Sanada, and Y. Takeda, "Sensorless control strategy for salient-pole PMSM based on extended EMF in rotating reference frame," *IEEE Trans. Ind. Appl.*, vol. 38, no. 4, pp. 1054–1061, Jul./Aug. 2002.
[5] Z. Chen, M. Tomita, S. Doki, and S. Okuma, "An extended electromotive force model for sensorless control of interior permanent-magnet synchronous motors," *IEEE Trans. Ind. Electron.*, vol. 50, no. 2, pp. 288–295, Apr. 2003.
[6] S. Chi, Z. Zhang, and L. Xu, "Sliding-mode sensorless control of direct-drive PM synchronous motors for washing machine applications," *IEEE Trans. Ind. Appl.*, vol. 45, no. 2, pp. 582–590, Mar./Apr. 2009.
[7] Y. Zhao, W. Qiao, and L. Wu, "An adaptive quasi-sliding-mode rotor position observer-based sensorless control for IPMSMs," *IEEE Trans. Power Electron.*, vol. 28, no. 12, pp. 5618–5629, Dec. 2013.
[8] A. Khlaief, M. Bendjedia, M. Boussak, and M. Gossa, "A nonlinear observer for high-performance sensorless speed control of IPMSM drive," *IEEE Trans. Power Electron.*, vol. 27, no. 6, pp. 3028–3040, Jun. 2012.
[9] Y. Zhao, W. Qiao, and L. Wu, "Model adaptive reference system-based speed estimators for sensorless control of interior permanent magnet synchronous machines," in *Proc. IEEE Transp. Electr. Conf. Expo*, Jun. 2013, pp. 1–6.
[10] V. Utkin, J. Guldner, and J. Shi, *Sliding Mode Control in Electromechanical Systems*, 1st ed. New York, NY, USA: Taylor & Francis, 1999.
[11] A. Bartoszewicz, "Discrete-time quasi-sliding-mode control strategies," *IEEE Trans. Ind. Electron.*, vol. 42, no. 2, pp. 117–122, Apr. 1995.
[12] S. Janardhanan and B. Bandyopadhyay, "Multirate output feedback based robust quasi-sliding mode control of discrete-time systems," *IEEE Trans. Autom. Control*, vol. 52, no. 3, pp. 499–503, Mar. 2007.
[13] J. Liu, J. Hu, and L. Xu, "Sliding mode observer for wide speed range sensorless induction machine drives: Considerations for digital implementation," in *Proc. IEEE Int. Conf. Electr. Mach. Drives*, May 2005, pp. 300–307.
[14] Y. Zhao, W. Qiao, and L. Wu, "Oscillation mitigation for sliding-mode observers in sensorless control of interior permanent magnet synchronous machines," in *Proc. IEEE Transp. Electr. Conf. Expo*, Jun. 2012, pp. 1–6.
[15] C. Schauder, "Adaptive speed identification for vector control of induction motors without rotational transducers," *IEEE Trans. Ind. Appl.*, vol. 28, no. 5, pp. 1054–1061, Sep./Oct. 1992.
[16] F. Z. Peng and T. Fukao, "Robust speed identification for speed sensorless vector control of induction motors," *IEEE Trans. Ind. Appl.*, vol. 30, no. 5, pp. 1234–1240, Sep./Oct. 1994.
[17] F. Dezza, G. Foglia, M. Iacchetti, and R. Perini, "An MRAS observer for sensorless DFIM drives with direct estimation of the torque and flux rotor current components," *IEEE Trans. Power Electron.*, vol. 27, no. 5, pp. 2576–2584, May 2012.
[18] M. Cirrincione, A. Accetta, M. Pucci, and G. Vitale, "MRAS speed observer for high-performance linear induction motor drives based on linear neural networks," *IEEE Trans. Power Electron.*, vol. 28, no. 1, pp. 123–134, Jan. 2013.
[19] L. Harnefors and M. Hinkkanen, "Stabilization methods for sensorless induction motor drives—A survey," *IEEE J. Emerging Sel. Topics Power Electron.*, to be published.
[20] M. Tomita, T. Senjyu, S. Doki, and S. Okuma, "New sensorless control for brushless DC motors using disturbance observers and adaptive velocity estimations," *IEEE Trans. Ind. Electron.*, vol. 45, no. 2, pp. 274–282, Apr. 1998.
[21] W. Qiao, X. Yang, and X. Gong, "Wind speed and rotor position sensorless control for direct-drive PMG wind turbines," *IEEE Trans. Ind. Appl.*, vol. 48, no. 1, pp. 3–11, Jan./Feb. 2012.
[22] Y. Zhao, C. Wei, Z. Zhang, and W. Qiao, "A review on position/speed sensorless control for permanent-magnet synchronous machine-based wind energy conversion systems," *IEEE J. Emerging Sel. Topics Power Electron.*, vol. 1, no. 4, pp. 203–216, Dec. 2013.
[23] B. Farhang-Boroujeny, *Adaptive Filters Theory and Applications*, 1st ed. New York, NY, USA: Wiley, 1999.
[24] B. Shao and A. Emadi, "A digital PWM control for switched reluctance motor drive," in *Proc. IEEE Veh. Power Propuls. Conf.*, Sep. 2010, pp. 1–6.

Yue Zhao (S'10) received the B.S. degree in electrical engineering from the Beijing University of Aeronautics and Astronautics, Beijing, China, in 2010. He is currently pursuing the Ph.D. degree in electrical engineering from the University of Nebraska-Lincoln, Lincoln, NE, USA.

He was a Graduate Student Researcher in 2011 and 2012 and a Summer Product Engineering Intern in 2013 with John Deere Electronic Solutions, Fargo, ND, USA. He is the inventor of four U.S. patents pending in electric motor drives and the author of more than 20 papers in refereed journals and international conference proceedings. His current research interests include electric machines and drives, power electronics, and renewable energy systems.

Mr. Zhao is a member of Eta Kappa Nu. He was a recipient of the Best Paper Prize of the 2012 IEEE Transportation Electrification Conference and Expo.

Wei Qiao (S'05–M'08–SM'12) received the B.Eng. and M.Eng. degrees in electrical engineering from Zhejiang University, Hangzhou, China, in 1997 and 2002, respectively, the M.S. degree in high performance computation for engineered systems from Singapore-MIT Alliance, Singapore, in 2003, and the Ph.D. degree in electrical engineering from the Georgia Institute of Technology, Atlanta, GA, USA, in 2008.

He has been with the University of Nebraska-Lincoln (UNL), Lincoln, NE, USA, since 2008, where he is currently an Associate Professor with the Department of Electrical Engineering. He is the author or co-author of three book chapters and more than 120 papers in refereed journals and international conference proceedings. His current research interests include renewable energy systems, smart grids, microgrids, condition monitoring and fault diagnosis, energy storage systems, power electronics, electric machines and drives, and computational intelligence for electric power and energy systems.

Dr. Qiao is an Associate Editor of the IEEE TRANSACTIONS ON INDUSTRY APPLICATIONS and the IEEE JOURNAL OF EMERGING AND SELECTED TOPICS IN POWER ELECTRONICS, and the Chair of the Sustainable Energy Sources Technical Thrust of the IEEE Power Electronics Society. He was a recipient of the 2010 National Science Foundation CAREER Award, the 2010 IEEE Industry Applications Society Andrew W. Smith Outstanding Young Member Award, the 2012 UNL College of Engineering Faculty Research and Creative Activity Award, the 2011 UNL Harold and Esther Edgerton Junior Faculty Award, and the 2011 UNL College of Engineering Edgerton Innovation Award. He has received four Best Paper Awards from IEEE IAS, PES, and PELS.

Long Wu (S'02–M'07–SM'12) received the B.Eng. degree from Shanghai Jiao Tong University, Shanghai, China, in 1998, the M.S. degree from Marquette University, Milwaukee, WI, USA, in 2003, and the Ph.D. degree from the Georgia Institute of Technology, Atlanta, GA, USA, in 2007, all in electrical engineering.

He has been with Deere & Company, Moline, IL, USA, since 2007 and is a Staff Engineer leading advanced power electronics and motor control algorithm research and development for vehicle electrification with John Deere Electronic Solutions, Fargo, ND, USA. He has published more than 20 papers in referred journals and conference proceedings in general power electronics area. He holds six U.S. patents granted and more than 20 pending as the Primary Inventor. His current research interests include electric vehicle/hybrid electric vehicle, IPM drive, sensorless control, and machine/drive condition monitoring.

Dr. Wu is a Guest Associate Editor of the IEEE TRANSACTIONS ON POWER ELECTRONICS and the IEEE JOURNAL OF EMERGING AND SELECTED TOPICS IN POWER ELECTRONICS. He is serving in the IEEE Industry Applications Society IDC Award Committee. He has received many Deere Enterprise Innovation Awards.